Int. J. Solids Structures Vol. 23, No. 3, pp. 351–368, 1987
Printed in Great Britain.

0020–7683/87 $3.00 + .00
Pergamon Journals Ltd.

FLOW LOCALIZATION IN ELASTIC–PLASTIC MATERIAL DEVELOPING FROM STRESS-FREE SURFACE†

HIROSHI KITAGAWA
Department of Mechanical Engineering, Osaka University, 2-1 Yamada-oka, Suita, Osaka 565, Japan

and

HISASHI MATSUSHITA
Matsushita Electric Industrial Co., Ltd., 3-15 Yagumo-naka, Moriguchi, Osaka 570, Japan

(*Received* 7 *February* 1985)

Abstract—Localized shear band formation developing from a stress-free surface in a highly strained elastic–plastic material under plane strain is studied, taking effects of both geometrical and material factors into consideration. Two kinds of treatments are adopted concerning representation of the constitutive property of the material, that is, (1) using a phenomenological constitutive equation formulated on the basis of J2-flow, J2-kinematic and J2-deformation theories and (2) simulating a mechanical behavior of a polycrystalline material introducing an aggregate composed of a single crystal whose property is formulated on the basis of a slip theory proposed by Asaro *et al.* in which effects of finite deformation and rotation of the lattice are fully considered. Numerical analyses are carried out by a finite element method concerning occurrence of bifurcation in a uniformly deformed state and trace of strain localization which is induced by geometrical and material imperfection. It is pointed out that there exist some relations between appearance of the bifurcation and development of localization. From the results for the polycrystalline model it is shown how unevenness of the free surface grows and the shear band develops from an initial random inhomogeneous deformation field.

1. INTRODUCTION

The localization of plastic flow into a shear band characterizes a limiting state of essentially smooth deformation in ductile materials in fact and is often regarded as a precursor of ductile fracture[1]. The course of the localization resulting in shear band formation, however, is very complex, because various material and geometrical factors in macro- and/or microscopic scales influence them.

It has been predicted theoretically that in a body with stress-free surfaces, an inhomogeneous deformation with relatively short wavelength is possible near the surfaces at a highly strained state, which is known as the surface instability phenomenon[2–4]. On the other hand, it has been observed that in the metal which has a typical polycrystalline structure, surface unevenness (roughness) grows with increase of strain, the magnitude of which is nearly proportional to the strain subjected to and the length of variation (wavelength) of which corresponds to the size of the crystal grain[5, 6]. The surface roughness, however, is induced by microstructural inhomogeneity and its growth is stable, so that it may be independent of the surface instability phenomenon. Another mode of surface waviness appears at a considerably large strain and grows rapidly, the wavelength of which is several times as long as the size of the grain[5–7]. The occurrence of this inhomogeneous deformation may be closely related to the instability[4] and there is certain evidence that this phenomenon acts as a trigger effect on the shear band formation appearing in a tensile thin plate[6].

In this paper, finite element analyses are carried out concerning occurrence and development of the localization in a plane strain block with two stress-free surfaces facing each other and subjected to uni-directional tension. The problems analyzed here are

† Presented at the XVIth International Congress of Theoretical and Applied Mechanics, 19–25 August 1984, Lyngby, Denmark.

determination of bifurcation points of various order appearing in a uniformly deformed state and visualization of bifurcation modes corresponding to them, and trace of growth of inhomogeneity developing from a slight initial geometrical imperfection and a material inhomogeneity. The latter analysis is intended to be performed as a numerical simulation of the whole process of localization, starting from diffused-type necking and developing into a shear band. On the basis of the obtained results it is discussed how the localized shear band is being built up under the presence of the free surface.

It is well known that the condition of localization which is predicted theoretically is influenced decisively by expression of the constitutive property[1, 8, 9]. It has been pointed out that a flow theory based on a smooth yield condition does not always give reasonable prediction for occurrence of shear flow localization. Allowance of tangential plastic flow to the yield surface or consideration of corner effect of the yield surface are significant[9]. The phenomenological corner theory[10, 11] is considered to be one of the best models for polycrystalline solids, which reflects discreteness of the slip mechanism of a crystal. It is, however, difficult to take the effects of the material inhomogeneity into account by this model. On the other hand, in the analysis of growth of localization, the situation is somewhat different such that deformation history in a pre-localized state influences significantly flow localization. A reasonable estimation of the deformation limit of a tensile thin plate can be obtained by a kinematic hardening theory[12] or a flow theory which is formulated from a smooth yield function for transversely isotropic material[13]. In this paper, two kinds of treatments concerning the constitutive equations are adopted, which are (1) using the phenomenological constitutive equation formulated on the basis of J2-flow, J2-kinematic and J2-deformation theories and (2) simulating the mechanical behaviors of a polycrystalline material introducing an aggregate of a single crystal whose mechanical properties are represented by the slip theory proposed by Asaro and co-workers[14, 15] in which effects of finite deformation and rotation of the lattice are considered.

2. COMPUTATIONAL PROCEDURE

2.1. *Problem statement*

The plastic strain localization which develops in a rectangular block with two parallel free surfaces under plane strain uniaxial tension is examined. The condition of loading ends is shear free and displacement in the normal direction prescribed, so that the block without any initial imperfection deforms homogeneously at the early stage and bifurcation points appear as deformation proceeds.

Figure 1 shows the models used in the analysis schematically. Besides the full model, named type (I), the sub-models types (II)–(IV) in Fig. 1 are used, among which the appropriate model is chosen corresponding to the dimension of localized deformation or wavelength of inhomogeneous deformation intended to be analyzed.

Three kinds of problems are analyzed, which are:

(1) distribution of the bifurcation points and calculation of their modes,

(2) growth of surface roughness or waviness developing due to the initial geometric or material imperfections, and

(3) occurrence and development of shear band penetrating into the body.

The type (II) and (III) models are used for bifurcation mode analyses of rather long and short wavelengths, respectively. Because the surface deformation appears with very short wavelength, a type (IV) model is adopted in the second problem. The analysis of the third problem is executed in regard to the region of type (I) or (II). A slight and smooth geometrical imperfection is given along the free boundary in the last two cases.

A finite element method which is formulated by a so-called updated Lagrangian description is used to solve the above problems. An appropriate region to be analyzed is divided by an eight-node rectangular element with four integration points. Thus, in order

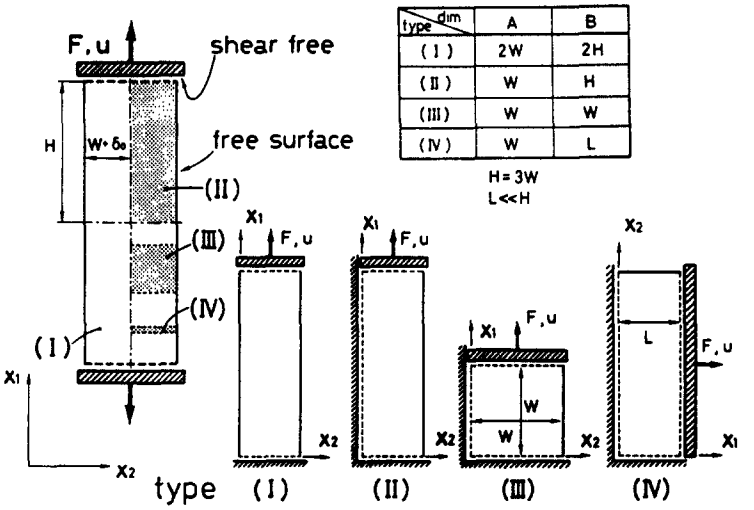

type \ dim	A	B
(I)	2W	2H
(II)	W	H
(III)	W	W
(IV)	W	L

Fig. 1. Models used in numerical analysis.

to avoid calculation errors due to the constraint of plastic incompressibility in the large strain, the reduced integration technique is adopted[16]. The standard incremental analysis with the increment of the boundary displacement prescribed is available. But it should be taken into account not only in calculating the kinematically accurate results at each step but also to avoid cumulation of the unbalanced forces even in the largely strained state.

2.2. *Constitutive equation*

The constitutive relations of elastic–plastic material are grouped into two categories, that is, those established from (1) a phenomenological point of view and (2) a physical point of view. The constitutive equations used in this paper are listed below, together with the fundamental basis of them.

A. *Phenomenological models*

(a) Flow theory which is formulated on the basis of isotropic hardening hypothesis and von Mises' yield function used as the plastic potential (J2-F material).
(b) Deformation theory formulated by the use of von Mises' yield function (J2-D material).
(c) Kinematic hardening theory founded on von Mises' yield function and Prager's proposal for its translation (J2-K material).

B. *Physical models*

(a) Single crystal model formulated by Asaro and co-workers[14, 15], on the basis of the slip theory.
(b) Polycrystalline aggregation model which consists of spatially distributed single crystals in random manner.

For all the cases except for the polycrystalline model, the constitutive equation can be expressed by the following rate type form with time-independent property

$$\overset{\nabla}{\tau}_{ij} = L_{ijkl} d_{kl} \tag{1}$$

where $\overset{\nabla}{\tau}_{ij} = \overset{\nabla}{\sigma}_{ij} + d_{kk}\sigma_{ij}$ is the Jaumann rate of Kirchhoff stress, $\overset{\nabla}{\sigma}_{ij}$ the one of the Cauchy stress, $d_{ij} = v_{(i,j)}$ the symmetric part of the velocity gradient, that is, the deformation rate tensor. L_{ijkl} is the fourth-order tensor which is evaluated from the material properties and

deformation history and so on. In eqn (1) and hereafter notations with subscripts mean the component of the vector or tensor with reference to the spatially fixed Cartesian coordinate system and the standard summation convention rule is applied.

The concrete forms of L_{ijkl} are summarized below.

Phenomenological model

$$L_{ijkl} = \hat{\lambda}\delta_{ij}\delta_{kl} + 2\hat{\mu}\delta_{ik}\delta_{jl} - \frac{3\hat{\mu}\hat{s}_{ij}\hat{s}_{kl}}{\hat{\sigma}^2(1 + \hat{h}/2\hat{\mu})}$$

$$\hat{\lambda} = \frac{\hat{E}\hat{\nu}}{(1 + \hat{\nu})(1 - 2\hat{\nu})}, \qquad \hat{\mu} = \frac{\hat{E}}{2(1 + \hat{\nu})}. \tag{2}$$

J2-F material

$\hat{\lambda}, \hat{\mu}$: Lame's constants

($\hat{E} = E$: Young's modulus, $\hat{\nu} = \nu$: Poisson's ratio)

$$\hat{s}_{ij} = \sigma_{ij} - \frac{1}{3}\sigma_{kk}\delta_{ij}, \qquad \hat{\sigma} = \sqrt{\left(\frac{2}{3}s_{ij}s_{ij}\right)}$$

$\hat{h}$: a scalar function which can be determined by the uniaxial true stress and natural strain curve as

$$\hat{h} = \frac{2}{3}\frac{2(1 + \nu)E_t}{2(1 + \nu) - E_t - (1 - 2\nu)} \tag{3}$$

where E_t is the tangent modulus.

J2-D material

$\hat{E} = E_s$: the secant modulus of the stress–strain curve

$$\hat{\nu} = \nu_s = E_s\left\{\frac{\nu}{E} + \frac{1}{2}\left(\frac{1}{E_s} - \frac{1}{E}\right)\right\},$$

$$\hat{h} = \frac{2}{3}\frac{E_sE_t}{E_s - E_t} \tag{4}$$

and all other quantities are the same as in J2-F.

J2-K material

$$\hat{s}_{ij} = t_{ij} - \frac{1}{3}t_{kk}\delta_{ij}, \qquad t_{ij} = s_{ij} = \Xi_{ij}$$

$\hat{\sigma} = \sigma_y$: the initial yield stress

Ξ_{ij}: the center of the yield surface in the stress space which is evaluated by

$$\overset{\nabla}{\Xi}_{ij} = \Xi_{ij} - \omega_{ik}\Xi_{kj} + \Xi_{ik}\omega_{kj}$$

$$= \frac{3}{2}\frac{1}{\sigma_y^2}(\overset{\nabla}{s}_{kl}\hat{s}_{kl})\hat{s}_{ij}, \qquad \omega_{ij} = v_{[i,j]}$$

$\hat{h}$: the scalar function given by eqn (3) but the equivalent stress should be calculated by the following equation (cf. Ref. [17]):

$$\sigma_y + \bar{\Xi}, \qquad \bar{\Xi} = \int\sqrt{\left(\frac{2}{3}\overset{\nabla}{\Xi}_{ij}\overset{\nabla}{\Xi}_{ij}\right)}\,dt. \tag{5}$$

Physical model

Slip theory of single crystal

Asaro and co-workers presented a constitutive representation of a single crystal, taking the distortion and rotation of the crystal grid due to finite deformation into account[14, 15]. Their formulation is convenient in an incremental analysis using the finite element method because it is expressible in the same form as eqn (1), in which L_{ijkl} is evaluated as

$$L_{ijkl} = E_{ijkl} - \sum_{\alpha=1}^{M}\sum_{\beta=1}^{M}(N^{-1})_{(\alpha\beta)}(P_{mn}^{(\alpha)}E_{mnij} + \beta_{ij}^{(\alpha)})(P_{st}^{(\beta)}E_{stkl} + \beta_{kl}^{(\beta)})$$

where M is the number of the active slip systems

$$P_{ij}^{(\alpha)} = \frac{1}{2}(s_i^{(\alpha)}m_j^{(\alpha)} + m_i^{(\alpha)}s_j^{(\alpha)})$$

$$W_{ij}^{(\alpha)} = \frac{1}{2}(s_i^{(\alpha)}m_j^{(\alpha)} - m_i^{(\alpha)}s_j^{(\alpha)})$$

$sm_i^{(\alpha)}$, $m_i^{(\alpha)}$ are the slip direction and normal to the slip plane of the α-slip system in the deformed state

$$N_{(\alpha\beta)} = h_{(\alpha\beta)} + (P_{ij(\alpha)}E_{ijkl} + \beta_{kl(\alpha)})P_{kl(\beta)}$$

$$\beta_{ij(\alpha)} = W_{ik(\alpha)}\sigma_{kj} - \sigma_{ik}W_{kj(\alpha)}$$

$$E_{ijkl} = \lambda\delta_{ij}\delta_{kl} + 2\mu\delta_{ik}\delta_{jl}$$

$h_{(\alpha\beta)}$ is the hardening rate of the α-slip system due to activation of the β-slip system, which is assumed to be expressed for L_{ijkl} to be symmetrized as

$$h_{(\alpha\beta)} = H_{(\alpha\beta)} + \frac{1}{2}(\beta_{ij(\beta)}P_{ij(\alpha)} - \beta_{ij(\alpha)}P_{ij(\beta)})$$

$$H_{(\alpha\beta)} = qH + (1-q)H\delta_{\alpha\beta}. \tag{6}$$

Polycrystalline model

Mechanical behavior of a polycrystalline material is directly simulated by constructing a heterogeneous aggregation of the single crystal introduced above. The constitutive properties of this model cannot be expressed in mathematical formulation explicitly in overall form, but the mechanical behavior of each model crystal grain is described by eqn (6). The elemental model crystal, to which a different slip system is assigned to each other, is constructed by several finite elements in order to allow the possibility of inhomogeneous deformation within the crystal grain.

3. BIFURCATION ANALYSIS

In a block without any imperfection, bifurcation points from a uniformly stretched state to a non-homogeneous deformation appear after the maximum axial force (the maximum load), at which the determinant of the incremental stiffness matrix of the finite element model (denoted by $\det K$) changes its sign. The succession of equilibrium states on which deformation pattern is essentially the same as the one before the maximum load is named fundamental deformation path (abbreviated as f.d.p.).

On an f.d.p. there are a lot of bifurcation points, to each of which a distinguishable

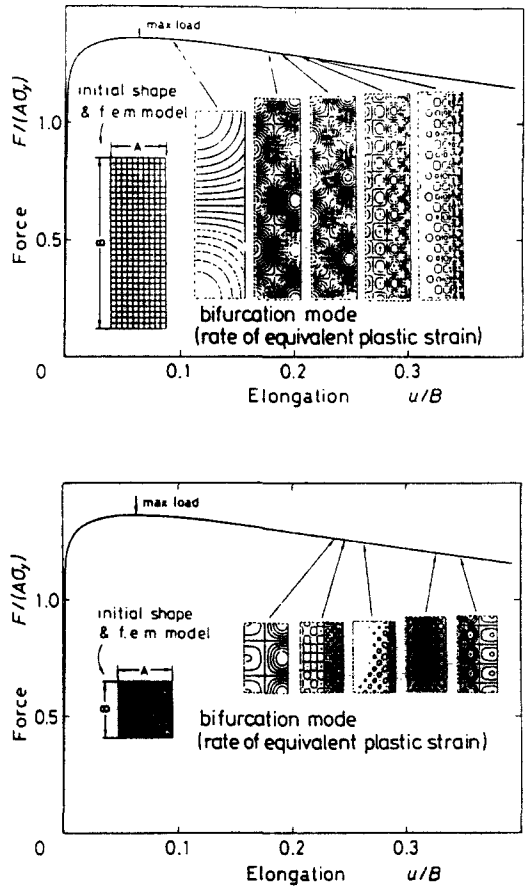

Fig. 2. Bifurcation points and modes (J2-D material, power law).

bifurcation mode corresponds. Figure 2 shows the bifurcation points and the bifurcation modes on the f.d.p. calculated for J2-D material. The uniaxial stress–strain relation used is the power law of hardening which is expressed as follows.

Type 1 hardening rule:

$$\varepsilon^{\mathrm{p}} = (\sigma_{\mathrm{y}}/E)(\sigma/\sigma_{\mathrm{y}})^{n} - \sigma/E$$
$$E = 200\,\mathrm{GPa}, \qquad \sigma_{\mathrm{y}} = 400\,\mathrm{MPa},$$
$$\nu = 0.3, \qquad n = 16. \tag{7}$$

In Fig. 2 the characteristic (bifurcation) modes expressed by equivalent plastic strain rate are shown with corresponding bifurcation points on the f.d.p. As recognized from its mode, the bifurcation point just after the maximum load is closely related to the occurrence of the diffused type necking with the longest wavelength. Observing the transition of the bifurcation mode it may be guessed to some extent how local inhomogeneous deformation occurs and develops. Figure 2(b) shows the results obtained by calculation which has been carried out for the purpose of extraction of the higher order (short wavelength) bifurcation mode, using a region with a small aspect ratio.

It should be noted that the amplitude of the rate of equivalent plastic strain in a higher order bifurcation mode varies with x_2 (through thickness) and as long as the longitudinal strain is less than a certain value, it decays toward the interior and its decay rate increases as the wavelength of the bifurcation mode becomes shorter. After the longitudinal strain exceeds some value the modes with reversed tendency appears, which should be worth noticing because this implies an appearance of a degree of freedom of

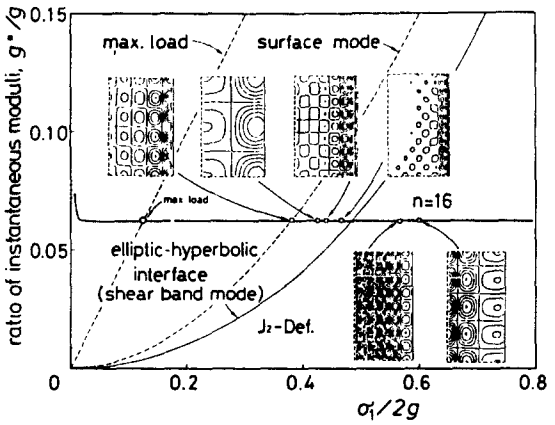

Fig. 3. Bifurcation points on the g^*/g–$\sigma_1/2g$ plane (J2-D material, power law).

internally localized deformation.

In Fig. 3 the same results as in Fig. 2 are plotted on the $g^*/g - \sigma_1/2g$ plane, where g and g^* are instantaneous moduli for shearing parallel to and at 45° to the tensile direction, respectively, and σ_1 is true tensile stress. For incompressible, time-independent incrementally linear solids, the conditions at which the maximum load, the surface mode (infinitesimally short wavelength) bifurcation point and the localized flow in shear band form (this means elliptic-hyperbolic interface of the governing differential equation) occur in the plane strain block under uniaxial tension were given by Hill and Hutchinson[3]. Their prediction is plotted in Fig. 3.

Comparing the numerical results with Hill and Hutchinson's prediction, the following correspondence is found. The f.d.p. traces the solid curve in Fig. 3 and the maximum load point on it almost coincides with Hill and Hutchinson's prediction, even if elastic compressibility is considered in the numerical calculation. The short wavelength mode of the bifurcation which has an uneven pattern of distribution concentrating remarkably toward the free surface appears about the intersection of the surface mode curve and the f.d.p. On the other hand, a localized-in-the-body mode appears after intersecting the elliptic–hyperbolic interface.

Such a transition of the bifurcation modes implies that the plastic strain localization in a body like a thin plate whose mechanical character is strongly influenced by existence of the surface seems to develop as follows: a diffused necking proceeds at first near the maximum load and then a short wavelength deformation whose magnitude decays rapidly with distance from the surface appears, which has been observed really as a sudden growth of surface roughness, and finally as soon as some degree of freedom for local deformation in the body is brought about, perhaps at the most deformed site produced by diffused necking, a shear band develops into the body.

The results obtained by the same calculation for the single crystal model are shown in Fig. 4. Hardening of the slip system is assumed to obey the following rule which was presented by Peirce *et al.* on the basis of the experimental data[15]

$$H(\gamma) = \frac{d\tau(\gamma)}{d\gamma}, \qquad \tau(\gamma) = \tau_0 + (\tau_s + \tau_0)\tanh\{H_0\gamma/(\tau_s - \tau_0)\}$$

$$H_0 = 8.9\tau_0, \qquad \tau_s = 1.8\tau_0, \qquad \tau_0 = 60.84\,\text{MPa},$$

$$q = 1, \qquad E = 1000\tau_0, \qquad \nu = 0.3$$

$$\gamma = \sum_{\alpha=1}^{M} \gamma^{(\alpha)}, \qquad \gamma^{(\alpha)}\text{: shear strain of } \alpha\text{-slip system.} \tag{8}$$

The number of slip systems is supposed to be 10, that is, the crystal has five pairs of slip systems. Further, it is assumed that all the angles between adjacent slip planes are the

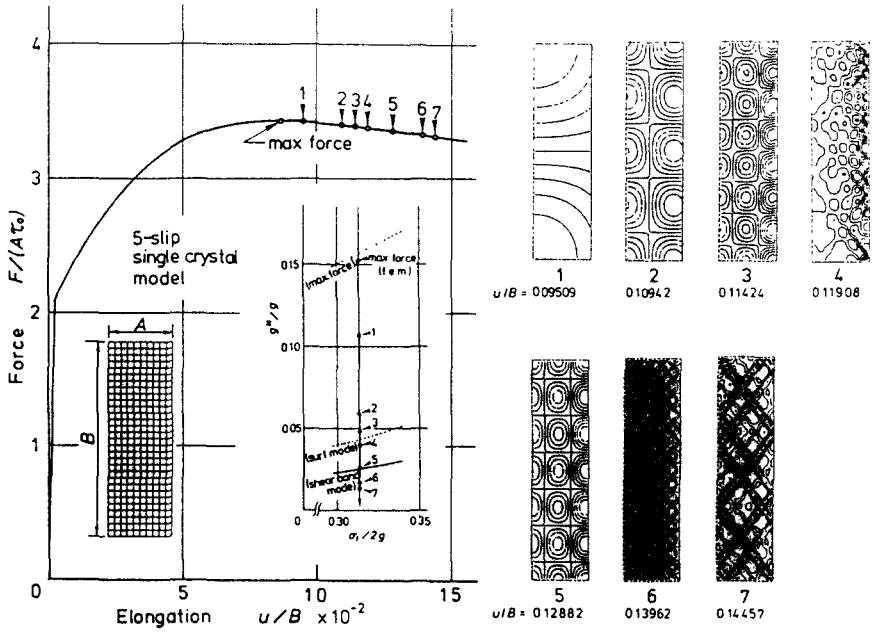

Fig. 4. Bifurcation points and modes appearing in a single crystal model.

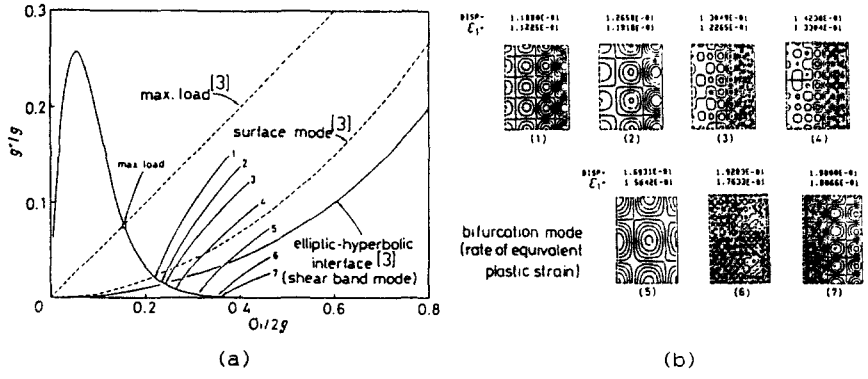

Fig. 5. Bifurcation points and modes (J2-D material, type 2 hardening rule).

same and are equal to 72° and one of them has the same direction as the tensile axis, thus all slip systems are symmetrically placed. This model is only fictitious and has no similarity with an actual crystal. The reason why such a construction of a slip system is adopted is that it is the simplest model which has a unique slip mode in the sense discussed by Peirce *et al.*[18], regardless of the direction of the crystal. But this fact has been confirmed only by numerical experimentation. The above property becomes important when a polycrystal model is constructed by a single crystal model. Although the material model is different from the previous case and that the trajectory tracing in the g^*/g–$\sigma_1/2g$ plane is dissimilar, the transitions of the bifurcation mode are similar. Bifurcation pattern No. 7 in Fig. 4 is somewhat different from the others. It was obtained merely by chance, but it should be worth noting that this pattern may not be a pure eigen mode but probably an interfering one with the shear band mode. Thus, appearance of the shear band mode is quite seldom, because it appears only when the aspect ratio of the region takes some special values so that the shear band transverses uniformly the whole region. This means that the shear band mode is local only in its width but not along its length.

In Fig. 5, the bifurcation behavior calculated for the J2-D material model whose hardening property is described by:

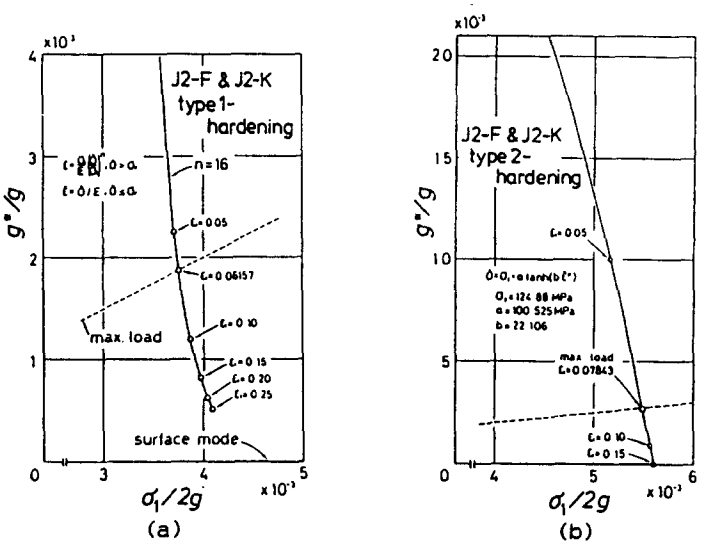

Fig. 6. Trajectories of fundamental deformation path on the g^*/g–$\sigma_1/2g$ plane: (a) J2-F and J2-K materials, type 1 hardening rule; (b) J2-F and J2-K materials, type 2 hardening rule.

Type 2 hardening rule:

$$\sigma = \sigma_y + \alpha \tanh(b\varepsilon^p)$$
$$\sigma_y = 124.88\,\text{MPa}, \qquad \alpha = 100.53\,\text{MPa},$$
$$b = 22.11, \qquad E = 1000\tau_0, \qquad \nu = 0.3,$$
$$\tau_0 = 60.84\,\text{kPa}. \tag{9}$$

The above relation is evaluated empirically so as to simulate the macroscopic stress–strain relation of the single crystal model. Changes of the bifurcation modes are essentially the same as the previous two cases but rather close to the last one. Comparing those two cases in some detail, it is found that the appearance of the higher order mode is considerably faster in the single crystal model than in the J2-D model, even if the stress–strain relation is the same in both cases.

Lastly, the trajectories of f.d.p. obtained for J2-F and J2-K material models are shown in Figs 6(a) and (b), whose hardening rules are type 1 (eqn (7)) and type 2 (eqn (9)), respectively. The results for J2-F and J2-K material models agree exactly. There is a significant difference between the trajectories shown in Figs 6(a) and (b). The trajectory for the type 1 hardening rule does not intersect the surface mode bifurcation curve within a reasonable strain level, but the one for the type 2 hardening rule can reach it because the hardening rate of type 2 rapidly decreases and the value of g^*/g tends to zero in this case, and thus inhomogeneous deformation localized near the surface might develop.

4. GROWTH OF INHOMOGENEOUS DEFORMATION NEAR THE SURFACE DEVELOPING FROM INITIAL IMPERFECTION—SIMULATION OF GROWTH OF SURFACE ROUGHNESS

In the plane strain block with a slight initial imperfection along the free surface, an inhomogeneous deformation appears in the early stage of deformation. To analyze the growth of this deformation one needs to examine an equilibrium state near f.d.p. and to understand the observed process of localization. In this section, the localization with a short wavelength mode which develops in a narrow region in the tensile direction is analyzed and the relation to the surface instability is discussed. The analyzed region is a type (IV) sub-model shown in Fig. 1 with a depth–width ratio $A/B = 10$ and an initial imperfection along the free surface expressed by

$$\delta_0 = \bar{\delta}_0 \cos(2\pi x_1/L), \qquad \bar{\delta}_0/L = 0.002. \tag{10}$$

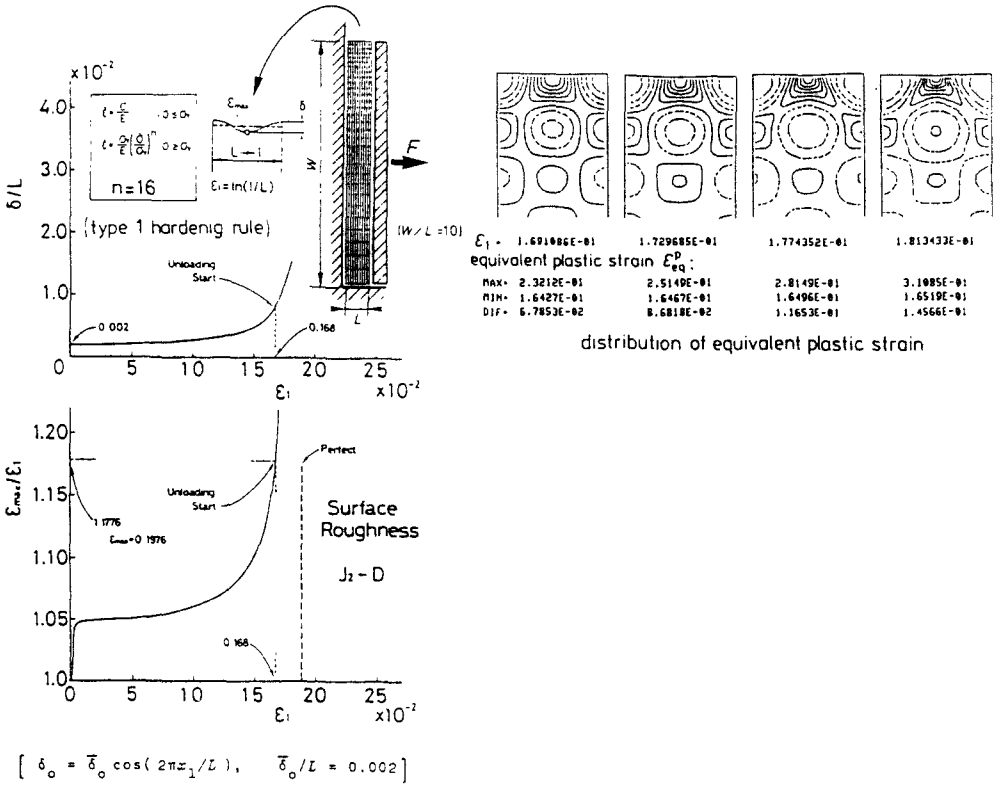

Fig. 7. Growth of surface unevenness and strain distribution near free surface: (a) growth of surface unevenness; (b) maximum strain in tensile direction; (c) distribution of equivalent strain near free surface.

4.1. *Growth of surface roughness in phenomenological and single crystal models*

The surface deformation of the J2-D material with type 1 hardening rule undergoes a change shown in Fig. 7. The path of the strain in the strain space deviates only slightly from a proportional one even in the most severely deformed portion and at the final stage shown in Fig. 7. Then, judging from comparison with the results of the same problem using the J2-corner theory presented by Hutchinson and Tvergaard[4], the total loading state may be kept everywhere in the region, so that the above results based on J2-D theory might not lose its own validity.

The unevenness of the surface which has had the shape prescribed before deformation increases slowly until the longitudinal strain reaches a certain value. Just after the increase rate of the unevenness speeds up, elastic unloading regions appear near both the loading ends on the surface, and at the same time narrow bands in which strain is higher than in any other place develop from the center of the surface into the body with a preferred angle (in this case inclined about 50° to the tensile direction). Although the overall strain at which the elastic unloading starts ($\varepsilon_1 = 0.168$) is smaller than the bifurcation strain of the surface mode ($\varepsilon_1 = 0.189$), not only has the maximum strain considerably exceeded the latter value, but also the average strain in some area including the maximum strain point has already reached it. By the way, the bifurcation strain of the surface mode is approximately evaluated as the first bifurcation point appearing in the type (IV) region without imperfection.

The results obtained by the same analyses on J2-F, J2-K and J2-D materials having type 2 hardening rule are shown in Fig. 8(a) and the ones on the single crystal model in Fig. 8(b). In the latter case, Asaro's model is an ideal plane crystal with symmetric primary-conjugate slip systems the planes of which are oriented 30° to the tensile direction.

In the case of the single crystal model and J2-D material, the elastic unloading occurs at relatively small strain and the surface unevenness (roughness) grows rapidly. It is

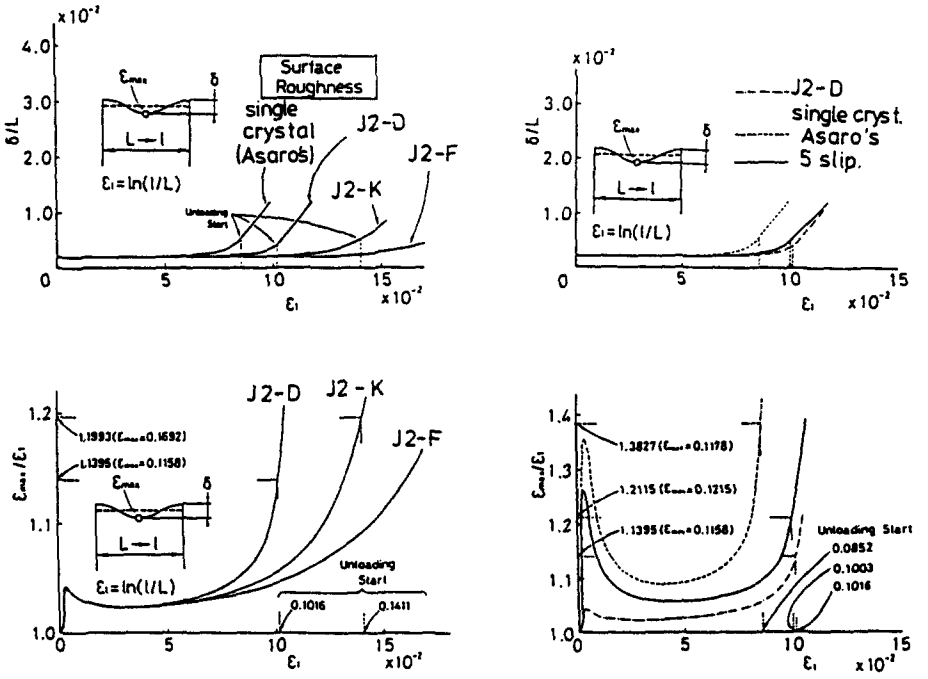

Fig. 8. Growth of surface unevenness developing in various material models.

interesting to note that the strains on the unloading for J2-D are close to those for the five-slip crystal model, which may correspond to the fact that the surface mode bifurcation strain for both cases is approximately the same (they can be estimated from Figs 4 and 5 as $\varepsilon_1 = 0.119$ for J2-D and 0.121 for the five-slip crystal), while changes of $\varepsilon_{max}/\varepsilon_1$ in the early stage are remarkably different.

As the hardening rate of the material with the type 2 rule decreases rapidly with increase of plastic strain, strain inhomogeneity proceeds considerably even in the case of J2-F material, but the unloading is not induced in this case. On the other hand, J2-K material reveals a remarkable growth of localized strain involving the elastic unloading, though both materials undergo the same behavior in the case of a perfect shaped body as pointed out previously.

Figure 9 shows the distributions of the equivalent plastic strain at the deformation stage when the increase of the surface roughness is accelerated. These figures indicate contour lines of the equivalent plastic strain. The interval of the strain between the adjacent contours is one-tenth of the difference between the maximum and minimum values of the strain in the whole region. The maximum and minimum values themselves are tabulated under each figure with the value of elongation. In the J2-D material, the two narrow deformation bands located symmetrically run into the body, making an angle of about 48.5° to the tensile direction, but formation of such a band cannot be recognized clearly in J2-F and J2-K materials. This deformation band will be called a shear band. The shear band formation proceeds earliest in Asaro's model of a single crystal, in which the band

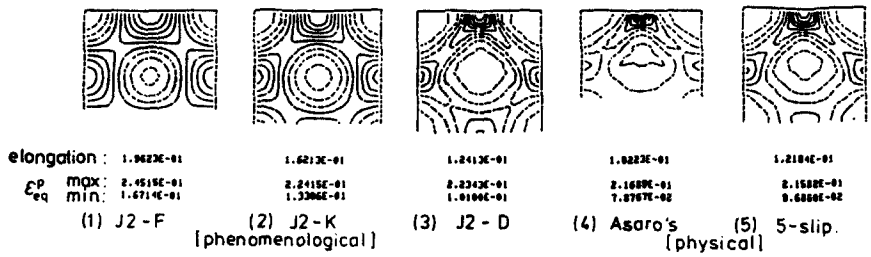

Fig. 9. Strain localization near the free surface developing in various material models.

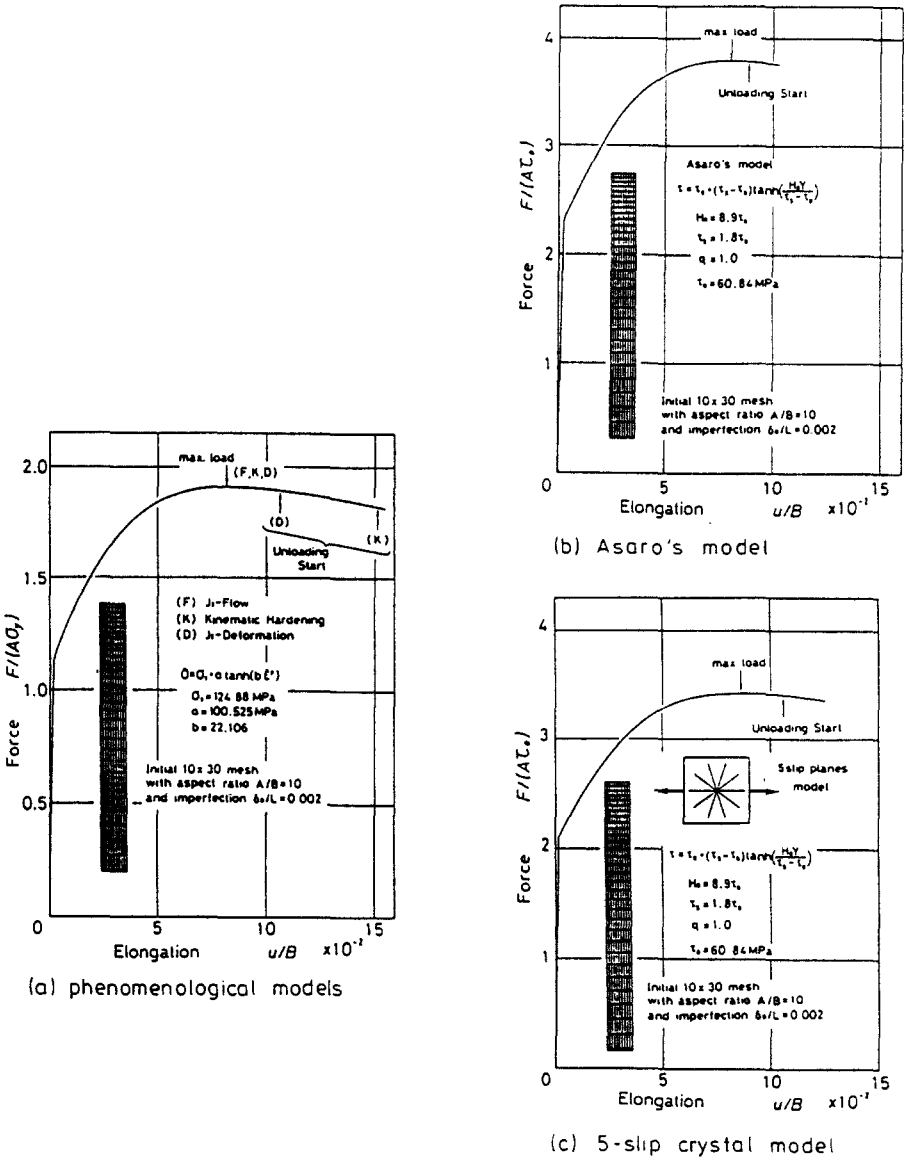

Fig. 10. Force–elongation curves and finite element meshes used in analysis of growth of surface unevenness (roughness).

also makes an angle of 48.5° near the surface but gradually turns its direction toward that of the slip plane of the crystal. On the other hand, though the five-slip model shows a similar behavior to Asaro's model in the early stage, its property concerning the formation of shear band comes to resemble the one of J2-D material. The above results should be worthy of attention, because they might indicate a certain appropriateness of the J2-D material model for analysis of the plastic instability problem involving localized strain.

In Fig. 10, force–elongation curves are shown with the finite element mesh pattern used in the above analyses. Comparing Fig. 10(c) with Fig. 4(a), it is seen that existence of the initial imperfection to the amount specified by eqn (10) does not influence the effect on the macroscopic behavior of the block. The curves of five-slip planes single crystal model gives smaller load than that of Asaro's model by about 10% for the same elongation. But this fact does not mean that there is some qualitative difference between them, because the maximum load point of both models occurs at approximately the same elongation.

4.2. *Growth of surface roughness developing in polycrystalline model*

According to the idea stated in Section 2.2, a polycrystalline model is constructed in the following way. A rectangular region intended to be analyzed with a depth–width ratio

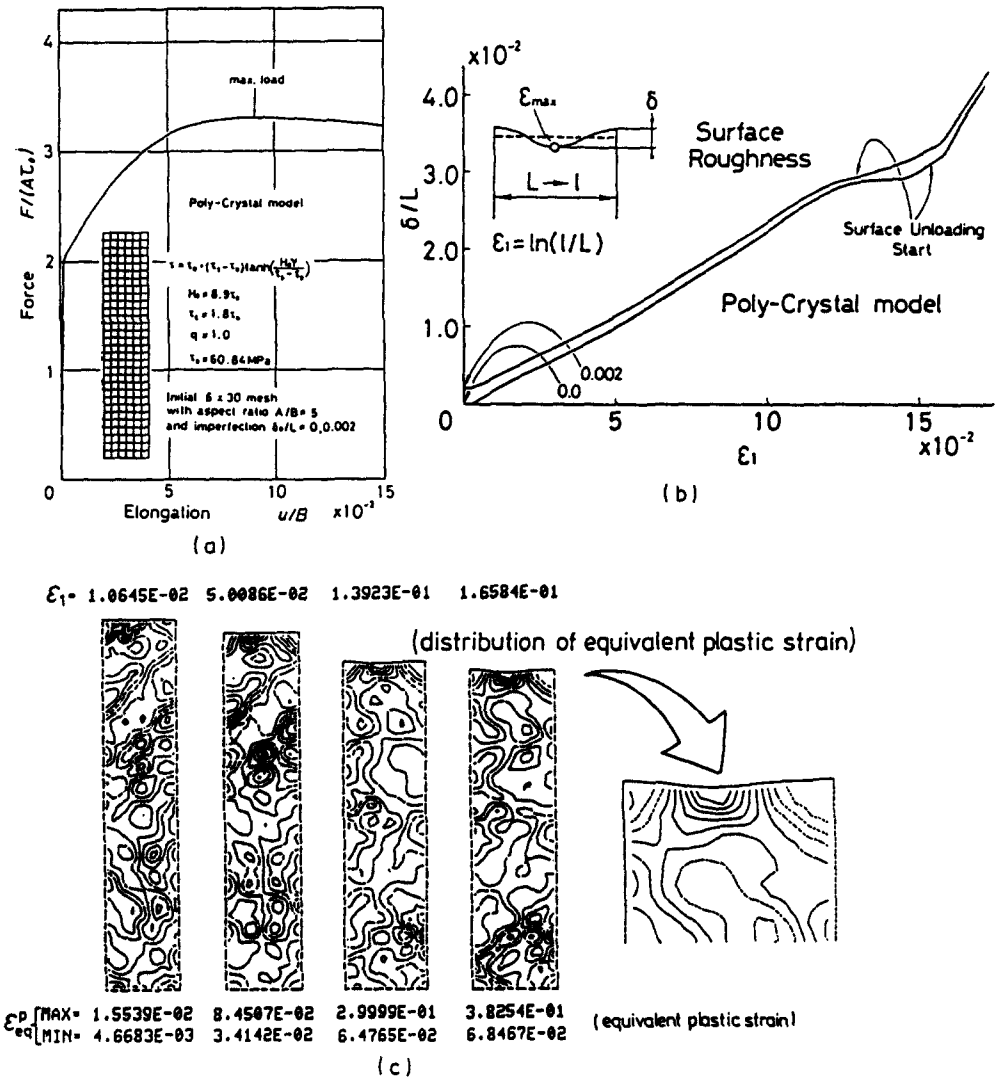

Fig. 11. Growth of surface roughness and development of localized deformation in a polycrystalline model: (a) force–elongation relation and finite element mesh; (b) growth of surface roughness; (c) changes of contour of equivalent plastic strain.

$A/B = 5$ is divided into 30 × 6 square finite elements. A collection of 2 × 2 finite elements is considered to correspond to a crystal grain, and thus, the whole region is modeled by an aggregation of 15 × 3 grains which are regularly arranged. Each grain is assumed to behave as a five-slip crystal model whose slip system has the prescribed random slip directions before deformation. In the polycrystalline model constructed in this way, inhomogeneous deformation occurs at the beginning of deformation, whether the initial geometrical imperfection exists or not, so that the effect of the existence of the imperfection may not be significant. To confirm this fact, both perfect and imperfect regions are taken to be analytical objections.

Figure 11(a) shows the load–elongation curve, which indicates that the macroscopic stiffness of this model is somewhat smaller than that of the five-slip crystal, in spite of using the same hardening rule. The surface roughness (unevenness) increases nearly in proportion to the strain from the beginning which is shown in Fig. 11(b). After an elastic unloading appears, its growth is accelerated. Before or after the occurrence of the unloading, the growth seems to stop in a short period. The existence of imperfection has no significant effect, as expected, and if the surface roughness–longitudinal strain curve for the perfect case is shifted upward by the amount of the initial imperfection, it almost coincides with the one for the imperfect case. As a whole, these results correspond well to the experimental

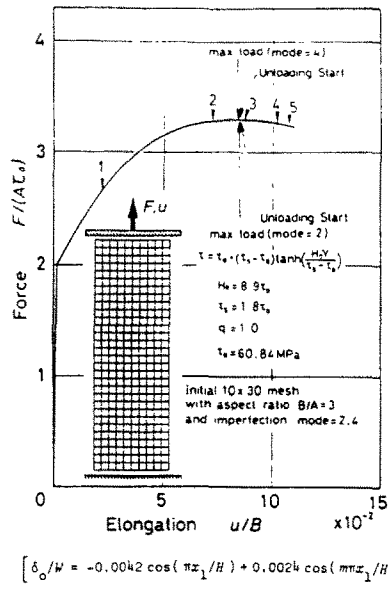

Fig. 12. Force–elongation curve and finite element mesh (uniaxial tension of polycrystalline model).

observations concerning the metal forming process of a thin plate.

Figure 11(c) shows changes of the distribution of the plastic equivalent strain as contour lines drawn in the same manner as in Fig. 9. The changes of the maximum and minimum values of the equivalent strain themselves should be noted. From these results, the transition of deformation inhomogeneity proceeds as follows: after a random non-uniform deformation is induced by the initial material structure in the very early stage, the deformation leaning toward the free surface proceeds and at the same time the surface roughness grows nearly proportional to the given strain. About the step when elastic unloading occurs, the strain within the body far from the surface increases and a shear band-like highly strained region appears near the surface and the surface roughness increases rapidly.

5. DEVELOPMENT OF SHEAR BAND PENETRATING INTO THE BODY

In this section a numerical analysis on the full region (Type (I) in Fig. 1) with a slight imperfection is carried out. No assumption concerning symmetry of deformation is imposed in order to investigate how the localization proceeds and how the shear band appears and develops from an all-round point of view.

The shape of the imperfection given initially to both free surfaces is expressed by

$$\delta_0/W = -0.0042\cos(\pi x_1/H) + 0.0024\cos(m\pi x_1/H),$$
$$m = 2 \text{ or } 4. \tag{11}$$

Numerical results obtained in the J2-D material and single crystal model cases are essentially the same as the results presented by Tvergaard *et al.*[19] and Needleman and Tvergaard[20], we devote our attention to examine the localization appearing in the polycrystalline model only.

The polycrystalline model is constructed in the same way as explained in Section 4.2. The whole region whose length–side ratio is $B/A = 3$ is divided into 30×10 square meshes and is considered to be made of 15×5 crystal grains, each of which is a five-slip model crystal, and has slip directions assigned randomly before deformation.

In Fig. 12 the force–elongation curve is shown together with the finite element model. Two kinds of initial imperfections (i.e. $m = 2$ and 4 in eqn (11)) are introduced, but the

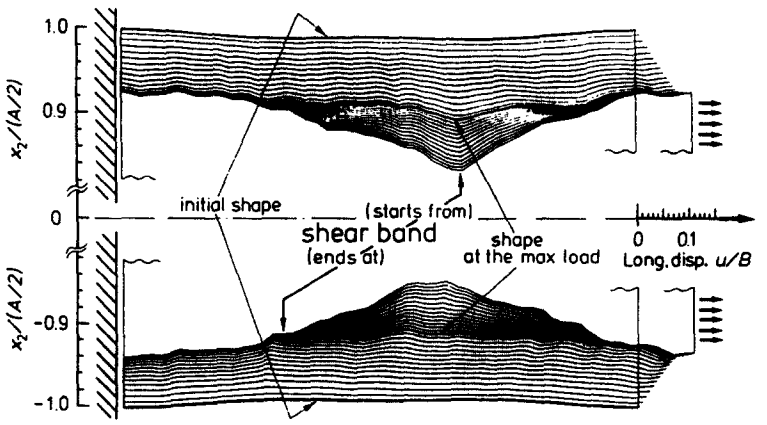

Fig. 13. Necking development (uniaxial tension of polycrystalline model).

results obtained in both cases almost coincide with each other. Thus, existence of long wavelength imperfection only (corresponding to the diffused necking mode) may be important in this case. The $m = 2$ case is discussed below. This force–elongation curve is almost the same as the one shown in Fig. 11(a), but the maximum load is attained at smaller elongation than in the previous case (Fig. 11(a)) and its difference is about 10%.

Figure 13 shows external shape changes, emphasizing the displacement components in the transverse (x_2) direction. As far as the change of external shape is observed, the necking seems to proceed in the following way: before the maximum force is attained, deformation is kept relatively uniform, but examined in detail, not only short wavelength unevenness increases with elongation but also diffused type necking is already growing. The former seems to be caused by the material inhomogeneity and the latter to the geometrical imperfection initially given. After the maximum force point, elastic unloading areas appear near both the loading ends and spread toward the central part. As deformation in the unloaded area actually ceases, then contraction of the width about the central part becomes remarkable. In order to observe this process in more detail, change of power spectrum of the surface unevenness is examined, which is shown in Fig. 14. It should be noted that the ordinate in this figure has a logarithmic scale. The longest wavelength component goes on growing with exponentially increasing rate. On the other hand, the

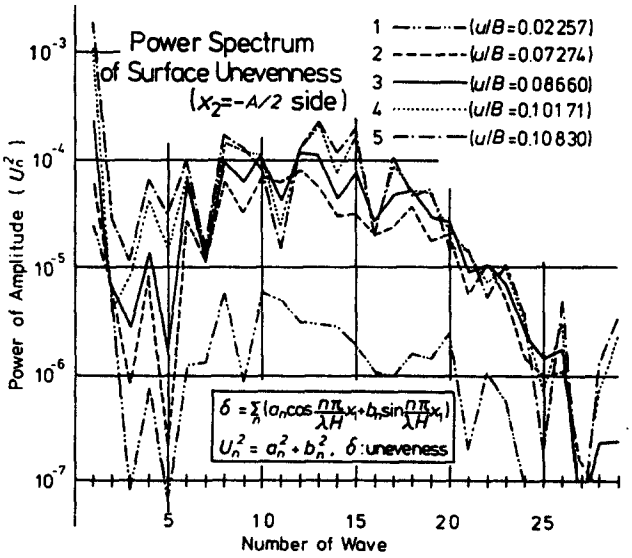

Fig. 14. Change of power spectrum of surface unevenness.

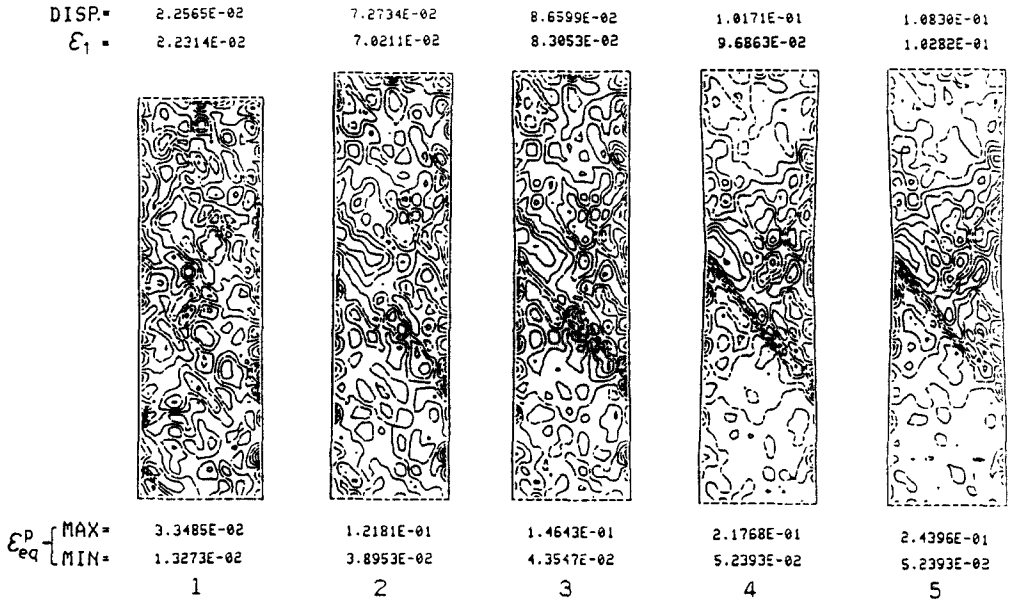

Fig. 15. Change of distribution of equivalent plastic strain and development of shear bands.

unevenness induced by crystal inhomogeneity which may be considered to correspond to the components of wave number between 8 and 20 seems to also increase collectively but it is not monotonical so that the pattern of the surface shape changes sometimes. It is worth noticing that increase of the components with the wave number 4, 5 after the maximum force point. The wavelength of these deformation components correspond to the dimension of the body in the transverse direction.

Turning our attention to changing of the distribution of strain in the body, Fig. 15 shows the transition of distribution of the plastic equivalent strain. The curves which mean contour lines of the plastic equivalent strain are drawn in the same way as those in Figs 5 and 11. The number attached to each figure corresponds to that of the force–elongation curve in Fig. 13. Figure number 3 indicates the state just after the maximum force point which is recognized clearly to be a turning point in the deformation pattern.

In very early step, inhomogeneity of deformation is considered to be uniform, reflecting the initially assigned microstructure, but even in figure number 1 a certain distinctive feature of the deformation pattern is already recognized, that is, nonuniformity of strain is strongest in the area near the free surface, and in the part along the center line of the width the nonuniformity is also remarkable. In Fig. 16, in which the maximum equivalent plastic strains which are found in the sections along the longitudinal lines of the Gaussian integration points of the finite element, which are normalized by division of the mean value, is shown, the curves corresponding to smaller elongation takes a W-shape, which indicates the above fact. In figure number 2 of Fig. 15 we can distinguish a deformation oriented in a preferred direction which seems to induce a shear band in the following step. The maximum strain already reaches that of the surface mode bifurcation at this stage.

At the maximum force point, a shear band penetrating the body is formed. Though the mean longitudinal strain is smaller than the bifurcation strain of a diffused mode for the five-slip crystal model (the first mode bifurcation occurs at $\varepsilon_1 = 0.09509$ as shown in Fig. 4), the maximum strain already exceeds the bifurcation strain of the shear band mode in the uniform deformation field.

After the maximum load, deformation becomes limited only within the central part and the diffused necking grows remarkably. On the other hand, a possibility of formation of shear bands with another direction (symmetrical to the previous one) appears in the body and growth of the diffused necking seems to be prompted by successive generations and development of the shear bands.

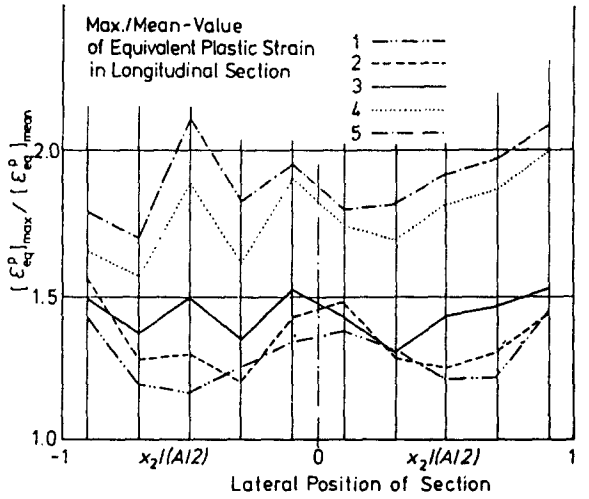

Fig. 16. Maximum equivalent plastic strain in longitudinal section.

6. CONCLUDING REMARKS

The localization of plastic flow is a widely observed phenomenon which seems to characterize a critical situation at which the body ceases to respond in the expected way. This phenomenon always involves mechanical instability and thus, nonlinearity is essential in nature. In order to understand the localization in itself, therefore, it is important to keep a general standpoint. That is, we should keep in mind that all kinds of mutual interactions among various factors which have any relations with this phenomenon, no matter how or what they are, can take an important role and a simple summation of effects due to each factor estimated separately does not always give a real description of it.

The results of the numerical analysis presented in this paper, especially concerning a model of the polycrystalline material, reproduce the essential features of the experimental observation. Initial geometrical imperfection, material inhomogeneity, discrete slip system, growth of surface roughness, surface deformation, diffused necking, elastic unloading, shear band formation, all these items are keywords to understand the localization developing in a polycrystalline material.

It has been shown that the plastic flow localization developing in a plane strain block subjected to uniaxial tension proceeds under mutual cooperation among the above items as follows: microscopically a heterogeneous structure of the material produces microscopically an inhomogeneous deformation field from a very early stage. In appearance, surface unevenness (roughness) increases steadily with increase of macroscopic strain. However, irregularity of deformation in the body is not uniform, but there are two parts in which the irregularity is greater than in others, that is, near the free surface and about the central part of the body. This peculiar deformation field has a decisive effect on the forthcoming instability macroscopically. On the other hand, a slight geometrical imperfection, especially one with long wavelength, promotes growth of diffused type necking. Cooperation of these two factors prepares situations at which a shear band starts from the surface, develops into the body and penetrates through it. Before the maximum load point this process is completed. After this point, the macroscopically deforming region shrinks as the elastic unloading region spreads and not only the localization of strain in the shear band becomes intensified, but also other shear bands are produced.

Although the localization proceeding in a block with free surfaces seems to be a smooth sequence of diffused type necking in appearance, the mechanism by which the macroscopic deformation is produced is quite different before and after the maximum load point. Thus, we can get effective information for better understanding the localization phenomena from the numerical calculation presented in this paper. A numerical simulation, so to speak, may be one of the best methods to grasp the dominating causes for this phenomena.

Acknowledgement—The authors gratefully acknowledge support from the Ministry of Education, Science and Culture of Japan, under Grand-Aid for Scientific Research, Project No. 57460076.

REFERENCES

1. J. R. Rice, *Theoretical and Applied Mechanics* (Edited by W. T. Koiter), p. 207. North-Holland, Amsterdam (1976).
2. M. A. Biot, *Mechanics of Incremental Deformation*, p. 159. Wiley, New York (1965).
3. R. Hill and J. W. Hutchinson, *J. Mech. Phys. Solids* **23**, 239 (1975).
4. J. W. Hutchinson and V. Tvergaard, *Int. J. Mech. Sci.* **22**, 339 (1980).
5. K. Osakada and M. Oyane, *Trans. JSME* **36**, 1017 (1970), in Japanese.
6. T. Kobayashi and H. Ishigaki, *J. Japan Soc. Tech. Plas.* **15**, 197 (1974), in Japanese.
7. A. K. Tadros and P. B. Mellor, *Int. J. Mech. Sci.* **20**, 121 (1978).
8. J. W. Hutchinson, *Proc. 8th U.S. National Congr. Appl. Mech.*, p. 81 (1979).
9. A. Needleman and J. R. Rice, *Mechanics of Sheet Metal Forming* (Edited by D. P. Koistinen and N.-M. Wang), p. 237. Plenum Press, New York (1978).
10. M. Gotoh, *Trans. JSME, A* 1389 (1981), in Japanese.
11. J. Christoffersen and J. W. Hutchinson, *J. Mech. Phys. Solids* **27**, 465 (1979).
12. V. Tvergaard, The Danish Center for Appl. Math. & Mech., Report No. 131. Tech. Univ. Denmark (1978).
13. T. L. Bassani, J. W. Hutchinson and K. W. Neals, *Metal Forming Plasticity* (Edited by H. Lippmann), p. 1. Springer, Berlin (1979).
14. R. J. Asaro, *Acta Metall.* **27**, 445 (1979).
15. D. Peirce, R. J. Asaro and A. Needleman, *Acta Metall.* **30**, 1087 (1982).
16. O. C. Zienkiwicz, *The Finite Element Method*, 3rd Edn, p. 279. McGraw-Hill, New York (1977).
17. V. Tvergaard, *Int. J. Mech. Sci.* **20**, 651 (1978).
18. D. Peirce, R. J. Asaro and A. Needleman, *Acta Metall.* **31**, 1951 (1983).
19. V. Tvergaard, A. Needleman and K. K. Lo, *J. Mech. Phys. Solids* **29**, 115 (1981).
20. A. Needleman and V. Tvergaard, *Finite Elements, Special Problems in Solids Mechanics* (Edited by J. T. Oden and G. F. Carey), Vol. V, p. 94. Prentice-Hall, Englewood Cliffs, New Jersey (1984).